Reduction of a heme cofactor initiates N-nitroglycine degradation by NnlA

Authors: Kara A. Strickland,[1,‡] Ashley A. Holland, [1,‡] Alan Trudeau, [1] Ilana Szlamkowicz, [1] Melanie J. Beazley, [1] Vasileios A. Anagnostopoulos,[1] David E. Graham,[2] Jonathan D. Caranto[1,*]

[1]Department of Chemistry, University of Central Florida, Orlando, FL 32816

[2]Biosciences Division, Oak Ridge National Laboratory, Oak Ridge, TN 37831

[‡]These authors contributed equally to this work

*email: jonathan.caranto@ucf.edu

This manuscript has been authored in part by UT-Battelle, LLC, under contract DE-AC05-00OR22725 with the US Department of Energy (DOE). The US government retains and the publisher, by accepting the work for publication, acknowledges that the US government retains a non-exclusive, paid-up, irrevocable, world-wide license to publish or reproduce the submitted manuscript version of this work, or allow others to do so, for US government purposes. DOE will provide public access to these results of federally sponsored research in accordance with the DOE Public Access Plan (http://energy.gov/downloads/doe-public-access-plan)

Abstract

The NnlA enzyme from *Variovorax sp.* strain JS1663 degrades the linear nitramine *N*-nitroglycine (NNG)—a natural product produced by some bacteria—to glyoxylate and nitrite (NO_2^-). Ammonium (NH_4^+) was predicted as the third product of this reaction. A source of non-heme Fe^{II} was shown to be required for initiation of NnlA activity. However, it was unclear if this Fe^{II} was being used as a metallocofactor or a reductant. This study reveals that NnlA contains a *b*-type heme cofactor. Reduction of this heme is required to initiate NnlA activity. Reduction can occur either by addition of a non-heme Fe^{II} source or by reduction with dithionite. Therefore, Fe^{II} is not an essential substrate for holoenzyme activity. Data are presented showing that reduced NnlA (Fe^{II}-NnlA) can catalyze at least 100 turnovers. In addition, this catalysis occurred in the absence of O_2. Finally, NH_4^+ was verified as the third product, accounting for the complete nitrogen mass balance. Size exclusion chromatography showed that NnlA is a dimer in solution. Additionally, Fe^{II}-NnlA is oxidized by O_2 and NO_2^- and binds carbon monoxide (CO) and nitric oxide (NO). These are characteristics shared with PAS domains; NnlA was previously shown to exhibit homology with such domains. Providing further evidence, a structural homology model of NnlA was generated based on the structure of the PAS domain from *Pseudomonas aeruginosa* Aer2. The structural homology model suggested His^{73} is the axial ligand of the NnlA heme. Site-directed mutagenesis of His^{73} to alanine decreased the heme occupancy of NnlA and eliminated NNG activity, providing evidence that the homology model is valid. We conclude that NnlA forms a homodimeric heme-binding PAS domain protein that requires reduction for initiation of the activity.

Importance

Linear nitramines are potential carcinogens. These compounds result from environmental degradation of high-energy cyclic nitramines and as by-products of carbon capture technologies. Mechanistic understanding of the biodegradation of linear nitramines is critical to inform approaches for their remediation. The best understood biodegradation of a linear nitramine is NNG degradation by NnlA from *Variovorax sp.* strain JS 1663; however, it is unclear why non-heme iron was required to initiate enzymatic turnover. This study shows that non-heme iron is unnecessary. Instead, our study reveals that NnlA contains a heme cofactor, the reduction of which is critical for activating NNG degradation activity. These studies constrain the proposals for NnlA reaction mechanisms, thereby informing mechanistic studies of degradation of anthropogenic nitramine contaminants. In addition, these results will future work to design biocatalysts to degrade these nitramine contaminants.

Keywords

Nitramine, N-nitroglycine, enzymology, heme, PAS domain, biodegradation, nitrogen

Introduction

Cyclic and linear (or aliphatic) nitramines are contaminants in soil and groundwater. Cyclic nitramines, such as hexahydro-1,3,5-trinitro-1,3,5-triazine, the high-energy compound RDX, are components of military-grade explosives. In addition to being products of RDX degradation, linear nitramines are by-products of some carbon capture technologies, formed when amines react with NO_x in the gas stream (1, 2).

RDX is a persistent soil contaminant at several explosives training facilities and manufacturing sites (3-5). Acute exposure to nitramines results in violent convulsions (6). Furthermore, the United States EPA lists RDX as an emerging contaminant and possible carcinogen. For these reasons, degradation pathways of RDX and other cyclic nitramines are well studied (7-13). One such pathway is initiated by a cytochrome P450 homolog, originally isolated from *Rhodococcus rhodochrous* strain 11Y, called XplA (14, 15). This enzyme reductively degrades RDX (**Fig. 1A**) (15-18). Under anaerobic conditions, the products are formaldehyde, nitrite (NO_2^-), and the one-carbon nitramine methylenedinitramine (MEDINA). Under aerobic conditions, RDX degradation produces the linear nitramine 4-nitro-2,4-diazabutanal (NDAB) instead. A transgenic *Arabidopsis* strain expressing the RDX degradation enzyme, XplA, has been engineered as a promising soil bioremediation strategy for RDX (3, 19).

Linear nitramines exhibit less acute toxicity than cyclic nitramines, but they have been shown to be skin and eye irritants (20, 21). Of greater concern, they are potential carcinogens (22-26). Linear nitramines often occur with their nitrosamine analogs, many of which are well-studied and potent carcinogens. Nitramines appear to be metabolized in a similar fashion as nitrosamines; specifically, their metabolism is initiated by hydroxylation by cytochromes P450 (22, 27-33). These hydroxylated products then degrade to form formaldehyde or alkylating

agents, which are the proposed mutagenic agents. Linear nitramines are photostable (34). Therefore, biodegradation appears to be their main environmental degradation pathway. Understanding the mechanisms of linear nitramine biodegradation is necessary to inform effective bioremediation strategies and design new biocatalysts for this purpose.

Compared to cyclic nitramines, there is far less known regarding the biodegradation pathways and mechanisms of linear nitramines. Some linear nitramines produced by carbon capture, particularly those with hydroxyl functionalities, were shown to be biodegraded by bacterial samples from soil and water (35). The products of these degradations were not reported. Biodegradations of NDAB by the fungus *Phanerochaete chrysosporium* and the bacterium *Methylobacterium* sp. strain JS178 have been reported (36, 37). In both cases nitrous oxide (N_2O) was produced. Initiation of the *P. chrysosporium* degradation was attributed to a manganese peroxidase. The mechanism of this degradation is unclear, but accumulation of N_2O suggests it is initiated by cleavage between the 4N-3C bond of NDAB (**Fig. 1A**)

The best characterized linear nitramine biodegradation pathway is an enzymatic pathway that degrades the natural product *N*-nitroglycine (NNG). This linear nitramine is produced by some bacteria including *Streptomyces noursei* (38, 39). The physiological function of NNG is unknown, but it exhibits toxicity towards Gram-negative bacteria and plants (38, 40). In addition, *in vitro* experiments have shown that NNG inhibits the ubiquitous succinate dehydrogenase enzyme (41). *Variovorax* sp. strain JS 1663 was enriched by its ability to use NNG as a sole carbon and nitrogen source (42). An NNG lyase (NnlA) was discovered to be essential for this phenotype. *In vitro* assays of NnlA showed it degraded NNG, producing glyoxylate and NO_2^- (**Fig. 1B**). A second nitrogenous product remains unidentified but was predicted to be ammonium (NH_4^+). Previous characterization of NnlA showed no evidence for a redox cofactor,

114 such as a heme or flavin.(43, 44) Therefore, NH_4^+ as the final product was consistent with a
115 redox-neutral degradation pathway and the apparent lack of a redox cofactor requirement.
116 However, NnlA was shown to be homologous to PAS domain proteins, which typically bind
117 heme or flavin. Furthermore, initiation of activity for heterologously expressed, purified NnlA
118 required addition of ferrous ammonium sulfate ($[Fe(NH_4)_2(SO_4)_2]$). This Fe^{II} may have
119 reconstituted a non-heme iron-containing active site capable of activating dioxygen (O_2)—a
120 well-known role for non-heme iron sites(45). An iron-dependent redox-mediated NNG
121 degradation pathway by NnlA could be envisioned. To test this hypothesis, the role of Fe^{II} for
122 NnlA activity needs to be clarified.

123 The purpose of this study was to identify the role of Fe^{II} in NnlA activity. En route to solving
124 this question, we found that NnlA binds a heme cofactor. As with non-heme iron, heme cofactors
125 are well-established to enable O_2 activation (46). Alternatively, heme may enable a reductive
126 degradation pathway as observed for RDX degradation by XplA. We investigated the role of the
127 NnlA heme cofactor, fully characterized the nitrogen mass balance of NNG degradation by
128 NnlA, and the O_2-dependence of turnover. The cumulative data herein explains why Fe^{II} was
129 needed to initiate activity in the prior work and shows it is not essential for activity. Finally, we
130 provide evidence that NnlA shares several characteristics with heme-binding PAS domain
131 proteins. The results provide insight into the mechanism of linear nitramine degradation and will
132 aid in developing remediation strategies and engineering new enzymes for bioprocessing.
133
134
135 **Material and Methods**

General reagents and protocols. Isopropyl β-D-1-thiogalactopyranoside (IPTG) and 5-aminolevulinic acid (5-ALA) were purchased from GoldBio. NNG was purchased from AAblocks. General buffers and media components were purchased from Fisher Scientific or VWR. Stock dithionite concentrations were determined by UV-visible absorbance at 318 nm (ε_{318} = 8000 $M^{-1}cm^{-1}$). The nitric oxide generator PROLI-NONOate was purchased from Cayman Chemicals. Stocks of PROLI-NONOate were prepared by dissolving approximately 10 mg of PROLI-NONOate in 10 mM NaOH and quantified by measuring the absorbance at 250 nm (ε_{250} = 6500 $M^{-1}cm^{-1}$) or 252 nm (ε = 8400 $M^{-1}cm^{-1}$), respectively. NO gas was purified prior to use by bubbling into degassed 10 mM NaOH in a septum-sealed container. Buffers were degassed in septum-sealed glass bottles by 3x vacuum/N_2 gas purge cycles on a Schlenk line connected using a 22 G needle punctured through the septum. Water used for all solutions was of 18.2 MΩ·cm resistivity from a Barnstead Nanopure (Thermo Fisher Scientific). Solvents for LC-MS experiments were of at least HPLC grade and contained 0.1% *v/v* formic acid. Recombinant TEV protease was expressed and purified as previously described (47).

Mutagenesis of nnlA. Site directed mutagenesis of the *nnlA* gene was performed to produce the variant protein NnlA H73A. Primers were designed for an "Round-the-horn" mutagenesis (**Table S1**) (48). The standard protocol was performed using Phusion polymerase and an annealing temperature of 63°C. The ligated reaction mixture was transformed into competent *E. coli* DH5α cells and plated on terrific broth (TB) agar plate containing 0.1 g/mL ampicillin. Colonies were selected and used to inoculate 5-mL Luria Broth (LB) cultures with 0.1 g/mL ampicillin, which were grown overnight at 37 °C. DNA was extracted from these cultures and analyzed by DNA sequencing (GeneWiz) to verify the mutation.

Expression and purification of NnlA and variant. Gene expression and affinity purification of NnlA protein using the pDG708 expression vector was performed as previously described (42). Alternatively, NnlA could be expressed from T7 Express cells transformed with pDG750, which contains the *nnlA* gene with an N-terminal His_{10}-tag, which is codon-optimized for expression in *E. coli*. NnlA with high heme occupancy was expressed by growth of these transformants in 4 x 1-L flasks of TB with 0.1 g/L of ampicillin at 37 °C. At an OD_{600} of 2, the temperature was decreased to 20 °C and NnlA expression induced with 100 mg/L of isopropyl ß-D-1-thiogalactopyranoside (IPTG), 1 g/L of ferric ammonium citrate (FAC) and 0.8 g/L 5-aminolevulinic acid (5-ALA). The cultures were grown for another 24 hours. Cells were pelleted by centrifuge at 6353 *g* yielding 17 g/L of wet cell mass. The pellet was either lysed immediately or stored frozen at -60 °C.

Cells were lysed by resuspending the cell pellet in a 1:2 (*m*/*v*) ratio of cells to Ni-buffer A (100 mM Tris-HCl, 100 mM NaCl at pH 7.6). The cell suspension was sonicated at 20 % amplitude for 10 minutes (10 seconds pulse, 10 seconds pause) for 3 cycles on ice. The cell debris was pelleted in a centrifuge at 53,000 *g* yielding a clear cherry-brown lysate. His_{10}-NnlA was loaded on a Ni-NTA HTC column (GoldBio), washed with 2 column volumes of Ni-buffer A, and eluted using a 6 column-volume gradient of 0 to 100% Ni-buffer B (100 mM Tris-HCl, 100 mM NaCl, 1 M imidazole at pH 7.6). Reddish-brown fractions were evaluated for relative heme incorporation using the ratio of 412 nm to 280 nm based on UV-visible absorption spectra. We found that fractions with a ratio $A_{412}/A_{280} > 1.0$ had the highest heme occupancies. Therefore, these fractions were evaluated for purity using SDS-PAGE. Pooled fractions were buffer exchanged into Ni-buffer A. Concentrated protein was aliquoted into microcentrifuge tubes and stored at -60 °C. NnlA H73A was expressed and purified as described above.

NnlA characterization and spectroscopy. NnlA was quantified using a bicinchoninic acid assay (Thermo Scientific). Total heme and non-heme iron was quantified using a literature iron assay that allows for release and subsequent detection of heme-ligated iron (49). Non-heme iron was specifically quantified using a ferrozine assay (50). Differentiation of the bound heme type was determined using the pyridine hemochromagen assay (51). Dissolved metal concentrations were determined using a Thermo Fisher Scientific iCAP-Qc inductively coupled plasma mass spectrometer (ICP-MS) with QCell technology and operated in kinetic energy discrimination (KED) mode of analysis with helium as the collision gas. Calibration, internal, and quality control standards (Inorganic Ventures) were prepared in 2% (v/v) HNO_3 and calibration standards were prepared at concentrations of 1 to 1000 µg L^{-1} (ppb).

To characterize the oligomer state of NnlA. The His_{10}-tag was cleaved from NnlA using recombinant TEV protease as previously described (47). The His_{10}-NnlA was incubated with TEV protease at 4°C for 72 hours. The digested protein was passed over a 2-mL Ni-HTC (GoldBio) gravity column to separate the tag-free NnlA, remaining His_{10}-NnlA, His_7-TEV, and cleaved His_{10}-tag. The brown flowthrough containing tag-free NnlA was concentrated, and 500 µL was then passed over a Superdex TM200 10/300 GL analytical gel filtration column. The column was preequilibrated with 100mM Tris-HCl, 100 mM NaCl at pH 7.8 at a flow rate of 0.1 mL/min. A standard mass curve was generated by passing a premade BioRad Gel filtration standard (#1511901) and blue dextran.

UV-visible absorption spectra of NnlA oxidation states and gas-bound forms were collected in an anaerobic glovebox (Vacuum Atmospheres Co.) atmosphere using an Ocean Optics USB2000+ UV-visible absorption spectrometer. Samples containing 10 µM NnlA in degassed buffer were titrated with stock sodium dithionite until the 430 nm absorbance of Fe^{II} NnlA no

longer increased. The ferrous-carbon monoxide and ferrous-nitrosyl NnlA adducts were generated by addition of either CO gas or purified NO gas to an anaerobic sample of 10 μM Fe^{II} NnlA contained in a septum sealed quartz cuvette. Spectra of Fe^{II} NnlA reacted with NNG or NO_2^- were collected after reaction of 2.7 μM Fe^{II} NnlA with 133 μM NNG or nitrite. Single wavelength traces were collected by monitoring 415, 417, or 437 nm absorbance every 4.8 seconds for the duration of the reaction.

General LC-MS methods. LC-MS analysis was performed using an Agilent 1260 LC stack equipped with a Zorbax RX-C18 column (5 μm, 4.6 x 150 mm) and connected to an Agilent 6230 TOF mass spectrometer with electrospray ionization (ESI). Analyses used an isocratic mixture containing 65% water, 25% acetonitrile, and 10% isopropanol at a flow rate of 0.5 mL/min. The mass spectrometer was run in negative ion mode with a probe voltage of 4500 V and fragmentation voltage of 175 V. To monitor NNG and glyoxylate, extracted ion chromatograms were obtained at *m*/*z* 119.0 and *m*/*z* 73.0, respectively. Concentrations of NNG and glyoxylate in samples were determined using calibration curves of standards containing 65, 125, 250, 500, and 750 μM NNG or glyoxylate in 10 mM tricine buffer.

Nitrogen assays. Ammonium concentrations were determined using a glutamate dehydrogenase assay (Sigma-Aldrich) kit using the manufacturer's instructions. Nitrite concentrations were determined by reacting 100 μL aliquots of reaction sample with 50 μL of deoxygenated Griess reagent R1 (Cayman Chemical, 1% sulfanilamide in 5% H_3PO_4) followed by addition of 50 μL of deoxygenated Griess reagent R2 (Cayman Chemical, 0.1% napthylethylenediamine dihydrochloride in water). The NO_2^- concentration was determined by using the molar absorption coefficient of the Griess-treated sample (ε_{542} = 50 $mM^{-1}cm^{-1}$) or from a standard curve generated from reactions with known concentrations of NO_2^-.

Samples were analyzed by ion chromatography for nitrite and nitrate using a Dionex Integrion High-Pressure Ion Chromatography (ThermoScientific) equipped with a 4 mm anionic exchange column (IonPac AS20), suppressor (Dionex ADRS 600 Suppressor) and a conductivity detector, operated at constant voltage (4.0V). The sample loop was 20 µL and was first degassed in an internal oven at 30 °C and then carried through the column by 35 mM NaOH (ultrapure, carbonate free, Acros Organics). The elution times under the conditions studied were 4 min and 4.9 min for nitrites and nitrates, respectively.

Preparation of NNG decomposition stoichiometry samples. Stoichiometry samples were prepared in an anaerobic glovebox using degassed buffers. Samples containing 10 µM as-isolated ($NnlA_{as\text{-}iso}$) or Fe^{II} NnlA were mixed with 500 µM NNG as needed for each sample. The dithionite control was prepared by mixing 500 µM NNG with 10 µM $Na_2S_2O_4$. Reduced samples contained 10 µM $Na_2S_2O_4$, 10 µM $NnlA_{as\text{-}iso}$, and 500 µM NNG in 10 mM tricine buffer, pH 8. Samples reacted with O_2 were prepared in two parts: 250 µL of 1 mM NNG remained outside of the glovebox under oxic conditions, while 250 µL of reduced protein was prepared inside the anaerobic glovebox by mixing NnlA and $Na_2S_2O_4$ to a final concentration of 20 µM each. The 250 µL aliquot of protein was removed from the box and added quickly to the 250 µL aliquot of oxygenated NNG in buffer with a final concentration of 20 mM potassium phosphate and pH 7.2. Every sample prepared was incubated for 30 minutes regardless of conditions.

Results

Characterization of NnlA and its heme cofactor. Recombinant NnlA with an N-terminal protease-cleavable decahistidine tag (His_{10}-NnlA) was produced in *E. coli* T7 Express cells. The His_{10}-NnlA protein was purified from the lysate by a Ni-NTA column. The theoretical mass of

His$_{10}$-NnlA was calculated as 20,526 Da. While a monomer band was observed in the SDS-PAGE of protein purified by a Ni NTA column, several other higher molecular weight bands also appeared (**Fig. S1A**). These higher molecular weight bands have weights consistent with NnlA oligomers.

To determine the solution oligomerization state of NnlA, TEV protease-cleaved NnlA was analyzed using size exclusion chromatography in 10 mM Tris-HCl at pH 7.6 (**Fig. S1B**). The chromatogram of TEV-cleaved NnlA exhibited two peaks. The first peak elutes in the void volume suggesting a higher oligomer with apparent molecular mass of 200 kDa or greater. The second peak corresponds to a molecular mass of 44 kDa, which is consistent with an NnlA homodimer. There was no appearance of a monomer peak. The results suggested that NnlA is a homodimer in solution, with some of the NnlA appearing as a larger aggregate.

The UV-visible absorption spectrum of as isolated His$_{10}$-NnlA exhibited a feature centered at 412 nm consistent with the presence of heme (**Fig. 2**). Supplementing expression cultures with 5-aminolevulinic acid (5-ALA), a heme precursor, resulted in preparations with a 6-fold higher molar absorption coefficient at 412 nm. These results indicate that addition of 5-ALA increases the occupancy of heme in recombinant NnlA. These preparations routinely contained 0.87 ± 0.21 total Fe atoms per NnlA monomer (**Table S2**). By contrast, negligible non-heme iron was detected by ferrozine assay. UV-visible absorption of samples of NnlA and myoglobin treated with the pyridine hemochromagen assay were nearly identical (**Fig. S2**). These results are consistent with the binding of a *b*-type heme. Other transition metals were detected in His$_{10}$-NnlA samples by ICP-MS (**Table S3**). However, most of these were sub-stoichiometric compared to the protein and are not expected to bind specifically to the protein. Nickel concentrations were high and likely due to the use of the Ni-NTA column during purification

273 (52). As discussed above, amino acid sequence alignment shows that NnlA contains a PAS
274 domain. The dimerization of the monomer and binding of a heme cofactor are common traits of
275 these domains (43, 44, 53).

276 ***Reduced NnlA reacts with O_2, NO, and CO.*** The role of the heme cofactor in PAS domains is
277 often a sensor of redox environment or of gas molecules such dioxygen (O_2), or nitric oxide
278 (NO) (53-55). Therefore, we characterized the reactions of paramagnetic gas molecules with
279 reduced NnlA. Reduction of the NnlA heme was monitored by UV-visible absorption
280 spectrophotometry (**Fig. 3**). The as isolated His_{10}-NnlA exhibited a Soret feature at 413 nm with
281 broad absorbance in the 500–700 nm region including poorly resolved peaks near 502 and 636
282 nm. The absorption spectrum is reminiscent of Fe^{III} hemoglobin or myoglobin (56). Therefore,
283 the as isolated His_{10}-NnlA is hereafter termed Fe^{III}-NnlA. Reduction of the sample was achieved
284 by titration of Fe^{III}-NnlA with dithionite until the absorbance at 413 nm no longer decreased.
285 Alternatively, the protein could be reduced by addition of an excess of $Fe(NH_4)_2(SO_4)_2$ (**Fig. S3**).
286 Under either reduction condition, the resulting reduced sample exhibited a Soret band at 437 nm
287 and formation of a Q-band maximum at 560 nm. This spectrum of reduced NnlA resembles that
288 of Fe^{II} myoglobin (56). Therefore, these features are hereafter attributed to Fe^{II}-NnlA and are
289 achieved using dithionite as the reductant.

290 The reaction of O_2, CO, or NO with Fe^{II}-NnlA was monitored by UV-visible absorption
291 spectrophotometry. There were no noticeable changes in the UV-visible absorption spectra when
292 O_2, CO, or NO were added to Fe^{III}-NnlA (**data not shown**). By contrast, each of these gases
293 readily reacted with Fe^{II}-NnlA (**Fig. 3**). Exposure of 10 μM Fe^{II}-NnlA to air resulted in the loss
294 of Fe^{II}-NnlA absorption features with a concomitant rise in Fe^{III}-NnlA absorption features over

295 several minutes. The intensities of these features were decreased compared to those observed for
296 the protein prior to reduction (**Fig. 3A**), suggesting that the observed oxidation of Fe^{II}-NnlA by
297 O_2 destroys some of the heme. Optical features consistent with the Fe^{II}-O_2 were not observed,
298 but it is expected to be an intermediate en route to heme oxidation.

299 Addition of NO gas to a deoxygenated sample of Fe^{II}-NnlA resulted in immediate
300 appearance of new absorbance features at 421, 550, and 580 nm. This spectrum is consistent with
301 that for the ferrous-nitrosyl ($\{FeNO\}^7$ by Enemark-Feltham notation (57)) adduct of myoglobin
302 (**Fig. 3B**) (56). Meanwhile, addition of CO to Fe^{II}-NnlA causes appearance of new absorption
303 features at 425, 542, and 568 nm. This spectrum is similar to that of the CO adduct of myoglobin
304 (58), thereby indicating that Fe^{II}-NnlA binds CO (**Fig. 3C**).

305 ***NnlA activity requires heme reduction and does not require O_2.*** The NNG degradation activity
306 of heme-occupied Fe^{III}-NnlA was first tested. Samples containing Fe^{III}-NnlA and NNG were
307 analyzed with LC-ESI-MS to monitor for decomposition of NNG (*m/z* 119.0) and formation of
308 glyoxylate (*m/z* 73.0). Extracted ion chromatograms (EICs) monitoring these molecular anions are
309 shown in **Fig. 4**. These Fe^{III}-NnlA samples showed no evidence for NNG decomposition to form
310 glyoxylate, suggesting Fe^{III}-NnlA needs to be activated to exhibit activity. As shown above,
311 $Fe(NH_4)_2(SO_4)_2$—required to initiate activity in prior work—was able to reduce the NnlA heme.
312 Therefore, we posited that NnlA activity is dependent on reduction of the heme instead of the
313 presence of a ferrous iron source.

314 To test this hypothesis, Fe^{II}-NnlA was incubated with NNG. These samples were prepared in an
315 anaerobic glovebox test the need for O_2 for the reaction. Anaerobic samples containing 10 μM
316 Fe^{II}-NnlA and 500 μM NNG exhibited complete degradation of the NNG to form glyoxylate (**Fig.**

4). For comparison, samples containing only dithionite and NNG exhibited no degradation of NNG. This result showed that the NnlA heme needs to be in the Fe^{II} oxidation state to activate NNG decomposition activity. The need for reduction of the heme to initiate NnlA activity unambiguously showed that the heme cofactor is necessary for NnlA activity, and its appearance is not an artifact of recombinant expression. Furthermore, this activation could be achieved without the need for $Fe(NH_4)_2(SO_4)_2$.

These experiments also precluded the hypothesis that NNG degradation by NnlA proceeds by a reductive or oxidative pathway. First, 10 μM Fe^{II}-NnlA performed 50 turnovers under these conditions. This catalytic NNG degradation shows that electron transfer from the heme to the NNG is not necessary, and thereby eliminated the possibility of a reductive NNG degradation pathway. In addition, complete NNG degradation was observed in the absence of O_2. This result precluded the possibility that O_2 activation by the NnlA heme is required for NNG degradation. In fact, simultaneous addition of O_2 and NNG resulted in less NNG degradation, indicating O_2 inhibits the reaction. These combined observations strongly suggested that NNG degradation by NnlA is redox-neutral.

Determination of the nitrogen mass balance. To verify that NNG degradation by NnlA is redox neutral, we determined the mass balance of the NNG degradation. Samples containing 10 μM Fe^{II}-NnlA and 1000 μM NNG in 10 mM tricine buffer, pH 8 were prepared under anaerobic conditions and incubated at 20 °C for 30 minutes. In parallel, NNG and glyoxylate were analyzed by LC-ESI-MS, NO_2^- was quantified by Griess assay or ion chromatography, and NH_4^+ was assayed by a L-glutamate dehydrogenase coupled assay. The EICs showed that the NNG in these samples was completely degraded with concomitant appearance of 1210 ± 290 μM

glyoxylate, accounting for 100% of the carbon mass balance. Parallel analysis of nitrogenous products showed the appearance of 810 ± 40 μM NO_2^- and 1050 ± 100 μM NH_4^+ in these samples. Ion chromatography showed no evidence for the presence nitrate (**Table S4**), providing further evidence against NNG degradation proceeding by an oxidative pathway. The total nitrogen products accounts for 93% of the nitrogen mass balance. These results are consistent with the following reaction stoichiometry:

$$NNG + H_2O \rightarrow NH_4^+ + NO_2^- + \text{glyoxylate} \qquad \text{(equation 1)}$$

This reaction stoichiometry of NNG degradation by NnlA is redox neutral.

NO_2^- oxidizes Fe^{II} NnlA. Given that the reaction stoichiometry was consistent with a redox-neutral process, it was not expected that NNG would oxidize Fe^{II}-NnlA. However, samples containing 3 μM Fe^{II}-NnlA reacted with 133 μM NNG under anaerobic conditions resulted in oxidation of Fe^{II}-NnlA within several hours as monitored by UV-visible absorption spectrophotometry (**Fig. 5A**). The final spectrum of this reaction exhibited spectral features Q-band features consistent with formation of the heme $\{FeNO\}^7$ shown in **Fig. 3B.** This observation suggested NNG degradation resulted in formation of some NO, which subsequently bound to Fe^{II}-NnlA to form the observed heme-nitrosyl adduct. Heme centers are well known to reduce nitrite to NO (59); therefore, we posited that the product NO_2^- was responsible for oxidizing the heme center and not NNG.

Indeed, addition of 133 μM NO_2^- to 3 μM of Fe^{II}-NnlA under anaerobic conditions oxidized the protein to Fe^{III}-NnlA (**Fig. 5B**). We note that in this experiment, there is no evidence for formation of an $\{FeNO\}^7$ species. Nevertheless, the time course of oxidation of the Fe^{II}-NnlA center, monitored by the decrease in 437 nm, was nearly identical whether in the presence of

363 NO_2^- or NNG (**Fig. S4**). These combined results indicated that NO_2^-, a product of NNG
364 degradation, oxidized Fe^{II} NnlA to Fe^{III} NnlA, thereby inactivating the protein. In other words,
365 the data show that NnlA was product inhibited.
366
367 ***Structural homology model of NnlA.*** To date, there are no published crystal structure models of
368 NnlA. However, the accumulated evidence suggests that NnlA is a PAS domain protein. To
369 provide structural prediction of NnlA, we generated a structural homology model using SWISS-
370 MODEL (**Fig. 6**). The model was selected by first allowing SWISS-MODEL to self-select
371 recommended templates. Models were then generated on all structural templates containing a
372 heme cofactor, consistent with the experimentally observed heme in NnlA. This method resulted
373 in the generation of 17 structural models. Out of the 17 models, 16 were based on previously
374 characterized PAS domains including those from DOS, FixL, and Aer2 protein complexes. The
375 best generated model threaded the NnlA sequence onto the crystal structure of the cyanide (CN)-
376 bound PAS domain of *Pseudomonas aeruginosa* Aer2 (PDB ID: 3VOL) and had a GMQE score
377 of 0.31. All other models exhibited a GMQE score between 0.03 and 0.18.
378
379 We tested the homology model by generating an NnlA variant with decreased heme
380 occupancy. In *Pa* Aer2, the heme is coordinated by an axial histidine ligand (60). Overlaying
381 the NnlA structural homology model on the *Pa* Aer2 structure reveals that H73 of NnlA is in a
382 similar position as the axial histidine coordinated to the *Pa* Aer2 heme (**Fig. 6**). To validate the
383 structural homology model and H73A NnlA variant was generated by site-directed mutagenesis.
384 The variant protein recombinantly expressed and purified as described for wild-type NnlA. The
385 total iron concentration per monomer protein (0.35 ± 0.08 μM Fe/monomer) of the H73A NnlA

was less than half that for wild-type NnlA (**Table S2**). Furthermore, there is a large amount of non-heme iron in the H73A NnlA samples, suggesting that the total iron assay overestimates the heme occupancy. Regardless, the iron analyses suggest that the H73A mutation adversely affects the binding of the heme cofactor. This conclusion is supported by UV-visible absorption spectra, which showed that the purified H73A NnlA exhibited an 8-fold lower molar absorption coefficient at 410 nm that that of the wild-type NnlA (**Fig. 7**). Finally, the variant protein lacks NNG degradation activity. There is no difference in the amount of NNG or glyoxylate in samples of Fe^{II}-H73A NnlA compared to Fe^{III}-H73A NnlA samples incubated with NNG for 30 minutes (**Fig. S5**). The combined results validate the proposed heme binding site from the structural homology model of NnlA.

Discussion

The conclusions of the data presented above are summarized in **Scheme 1**. A critical first conclusion is that NnlA contains a heme cofactor that is essential for activity. First, supplementing cultures expressing NnlA with the heme precursor 5-ALA resulted in NnlA preparations that bound one *b*-heme per subunit (**Fig. 2, Table S2, and Fig. S2**). Reduction of the heme is required to initiate activity (**Fig. 4**). Finally, generation of the heme-depleted variant, NnlA H73A, results in loss of NNG degradation activity (**Fig. S5**).

A key goal of this study was to understand the need for an Fe^{II} source in the previous study. Without culture medium supplementation with 5-ALA, preparations of NnlA in the prior study had low heme occupancies (**Fig. 2**). While samples had enough heme-bound monomers to turnover NNG, the low occupancy precluded detection of the cofactor by UV-visible absorption spectroscopy. With the observation that $Fe(NH_4)_2(SO_4)_2$ reduced the NnlA heme (**Fig. S3**), it is

most likely that this Fe^{II} source reduced a small quantity of heme-bound NnlA, all of which was responsible for the observed activity. We conclude that initiation of NNG degradation by NnlA is dependent on reduction of the heme and does not require the presence of non-heme Fe^{II}.

Heme cofactors often mediate redox-dependent chemistries. For example, reductive degradation of the cyclic nitramine RDX is mediated by the heme cofactor of XplA (15-18). Furthermore, heme cofactors are well-established to activate O_2,(46) presenting the possibility of a high-valent iron-oxo species participating in NNG decomposition. However, our experiments showed that activity does not require O_2, precluding the possibility that O_2 activation is required for NNG degradation (**Fig. 4**). In fact, O_2 inhibited the NnlA-catalyzed decomposition of NNG (**Fig. 3**). Furthermore, Fe^{II}-NnlA can perform at least 100 turnovers (**Table 2**), indicating that NNG is not reduced during degradation. Finally, complete determination of the nitrogen mass balance verified NH_4^+ as the second nitrogenous product of NNG decomposition by NnlA (**Table 2**). The combined results are consistent with NNG degradation by NnlA being a redox-neutral process.

The finding of an essential heme for NnlA activity now requires further understanding of its specific role. As discussed above, NnlA is predicted to be structurally homologous with PAS domains. In addition, we have established that NnlA required a heme cofactor for activity. We characterized NnlA as a dimer (**Fig. S1B**), and PAS domain proteins are often dimers or tetramers in solution (44, 61). In addition, suggested templates for structural homology modeling by SWISS-MODEL were nearly all structures of PAS domain proteins. Finally, the NnlA heme is capable of binding CO and NO to form stable complexes (**Fig. 3**). The NnlA heme does not stably bind O_2 but is instead oxidized by O_2. However, the structural homology model predicts that a critical distal tryptophan residue that stabilizes O_2 binding in *Pa* Aer2 (60) is absent in

NnlA and is replaced with a glutamine residue (**Fig. 6**). This may account for the differing reactivity of the NnlA heme compared to those of previously characterized heme-binding PAS domains that are O_2 sensors. Regardless, the accumulated evidence supports assignment of NnlA as a PAS domain protein.

Typically, PAS domains are redox or O_2 sensor domains (43, 44, 53). Activation of the domains by change in oxidation state or binding of O_2 triggers downstream processes, such as kinase activity or chemotaxis. Therefore, one possibility is that the NnlA heme is a redox sensor that triggers organization of an allosteric active site for NNG degradation in NnlA (**Scheme 2**). Most PAS domain-containing subunits do not also contain the catalytic site. However, our results indicate that the NnlA monomer contains both the regulatory PAS domain as well as a catalytic domain. Alternatively, the active site may reside at the subunit interface thereby requiring oligomerization for activity. By this hypothesis, NnlA activity would be regulated by the redox environment, either by the presence of O_2 or NO_2^-. As shown in **Fig. 3**, O_2 oxidizes Fe^{II}-NnlA, which inactivates the enzyme. This observation is consistent with the observation of less NNG degradation in oxic samples (**Fig. 4**). The oxidation of NNG by NO_2^- (**Fig. 5**) indicates that NO_2^- could also act in a regulatory fashion as a product inhibitor.

A second hypothesis is that the Nnla heme is repurposed as an active site instead of a regulatory site and therefore, the heme directly participates in NNG degradation. It was previously proposed that a general base deprotonates the NNG α-carbon, thereby, promoting β-elimination of NO_2^- from NNG to form an imine (42). Subsequent hydrolysis of the imine intermediate results in formation of the degradation products NH_4^+ and glyoxylate. By our second hypothesis, the Fe^{II}-heme could act as a Lewis acid to activate the nitro group and

promote elimination of the NO_2^- (**Scheme 2**). Differentiating between these two hypotheses will be required to identify the active site and enable future engineering efforts.

While the physiological function and biosynthetic pathway of NNG is still unknown, the finding of an NNG-degrading enzyme suggests that it is present in some abundance in the environment. It was previously shown that NNG is a potent inhibitor of the metabolic enzyme succinate dehydrogenase.(41) Additionally, NNG is isolectronic with 3-nitropropionate, a potent toxin produced by some fungi and plants.(62) It is reasonable to posit that NNG acts in some antibiotic function and that NnlA is a nitramine detoxification enzyme. However, the observation that NNG degradation by NnlA is product inhibited (or by the redox environment) would be unusual for a detoxification enzyme. Further studies of the role of this molecule and the ecological function of NnlA are warranted. Future studies may engineer NnlA to degrade nitramines of environmental concern, leveraging the mechanistic insight from this work.

Acknowledgements

This research was made possible by funding from the United States Army Research Office under grant #W911NF2010286. We thank the UCF McNair Scholars Program for supporting the training and research of A.T. This work was supported in part by the Strategic Environmental Research and Development Program (SERDP) under project WP20-1151. Oak Ridge National Laboratory is managed by UT-Battelle, LLC, for the U.S. Department of Energy under contract no. DE-AC05-00OR22725. We also thank Dr. Matthew Rex and Bhavini Goswami for their assistance in LC–MS.

References

1. Låg M, Lindeman B, Instanes C, Brunborg G, Schwarze PE. 2011. Health effects of amines and derivatives associated with CO_2 capture. Norwegian Institute of Public Health, Norway.

2. Chen X, Huang G, An C, Yao Y, Zhao S. 2018. Emerging N-nitrosamines and N-nitramines from amine-based post-combustion CO_2 capture–a review. Chem Eng J 335:921-935.

3. Rylott EL, Jackson RG, Sabbadin F, Seth-Smith HM, Edwards J, Chong CS, Strand SE, Grogan G, Bruce NC. 2011. The explosive-degrading cytochrome P450 XplA: biochemistry, structural features and prospects for bioremediation. Biochim Biophys Acta Proteins Proteom 1814:230-236.

4. Rylott EL, Bruce NC. 2009. Plants disarm soil: engineering plants for the phytoremediation of explosives. Trends Biotechnol 27:73-81.

5. Jenkins TF, Bartolini C, Ranney TA. 2003. Stability of CL-20, TNAZ, HMX, RDX, NG, and PETN in moist, unsaturated soil. US Army Engineer Research and Development Center, Cold Regions Research and Engineering Lab Hanover, NH.

6. Burdette LJ, Cook LL, Dyer RS. 1988. Convulsant properties of cyclotrimethylenetrinitramine (RDX): spontaneous, audiogenic, and amygdaloid kindled seizure activity. Toxicol Appl Pharmacol 92:436-444.

7. Zhao J-S, Halasz A, Paquet L, Beaulieu C, Hawari J. 2002. Biodegradation of hexahydro-1, 3, 5-trinitro-1, 3, 5-triazine and its mononitroso derivative hexahydro-1-nitroso-3, 5-dinitro-1, 3, 5-triazine by Klebsiella pneumoniae strain SCZ-1 isolated from an anaerobic sludge. Appl Environ Microbiol 68:5336-5341.

8. Bhatt M, Zhao J-S, Halasz A, Hawari J. 2006. Biodegradation of hexahydro-1, 3, 5-trinitro-1, 3, 5-triazine by novel fungi isolated from unexploded ordnance contaminated marine sediment. J Ind Microbiol Biotechnol 33:850.

9. Fournier D, Halasz A, Thiboutot S, Ampleman G, Manno D, Hawari J. 2004. Biodegradation of octahydro-1, 3, 5, 7-tetranitro-1, 3, 5, 7-tetrazocine (HMX) by Phanerochaete chrysosporium: new insight into the degradation pathway. Environ Sci Technol 38:4130-4133.

10. Coleman NV, Nelson DR, Duxbury T. 1998. Aerobic biodegradation of hexahydro-1, 3, 5-trinitro-1, 3, 5-triazine (RDX) as a nitrogen source by a Rhodococcus sp., strain DN22. Soil Biol Biochem 30:1159-1167.

11. Zhao J-S, Paquet L, Halasz A, Hawari J. 2003. Metabolism of hexahydro-1, 3, 5-trinitro-1, 3, 5-triazine through initial reduction to hexahydro-1-nitroso-3, 5-dinitro-1, 3, 5-triazine followed by denitration in Clostridium bifermentans HAW-1. Appl Microbiol Biotechnol 63:187-193.

12. Crocker FH, Indest KJ, Fredrickson HL. 2006. Biodegradation of the cyclic nitramine explosives RDX, HMX, and CL-20. Appl Microbiol Biotechnol 73:274-290.

13. Balakrishnan VK, Halasz A, Hawari J. 2003. Alkaline hydrolysis of the cyclic nitramine explosives RDX, HMX, and CL-20: New insights into degradation pathways obtained by the observation of novel intermediates. Environ Sci Technol 37:1838-1843.

14. Seth-Smith HM, Rosser SJ, Basran A, Travis ER, Dabbs ER, Nicklin S, Bruce NC. 2002. Cloning, sequencing, and characterization of the hexahydro-1, 3, 5-trinitro-1, 3, 5-triazine degradation gene cluster from Rhodococcus rhodochrous. Appl Environ Microbiol 68:4764-4771.

15. Rylott EL, Jackson RG, Edwards J, Womack GL, Seth-Smith HM, Rathbone DA, Strand SE, Bruce NC. 2006. An explosive-degrading cytochrome P450 activity and its targeted application for the phytoremediation of RDX. Nat Biotechnol 24:216.

16. Halasz A, Manno D, Perreault NN, Sabbadin F, Bruce NC, Hawari J. 2012. Biodegradation of RDX nitroso products MNX and TNX by cytochrome P450 XplA. Environ Sci Technol 46:7245-7251.

17. Halasz A, Spain J, Paquet L, Beaulieu C, Hawari J. 2002. Insights into the formation and degradation mechanisms of methylenedinitramine during the incubation of RDX with anaerobic sludge. Environ Sci Technol 36:633-638.

18. Jackson RG, Rylott EL, Fournier D, Hawari J, Bruce NC. 2007. Exploring the biochemical properties and remediation applications of the unusual explosive-degrading P450 system XplA/B. Proc Natl Acad Sci USA 104:16822-16827.

19. Cary TJ, Rylott EL, Zhang L, Routsong RM, Palazzo AJ, Strand SE, Bruce NC. 2021. Field trial demonstrating phytoremediation of the military explosive RDX by XplA/XplB-expressing switchgrass. Nat Biotechnol:1-4.

20. Fjellsbø LM, Van Rompay AR, Hooyberghs J, Nelissen I, Dusinska M. 2013. Screening for potential hazard effects from four nitramines on human eye and skin. Toxicol In Vitro 27:1205-1210.

21. Wagner ED, Osiol J, Mitch WA, Plewa MJ. 2014. Comparative in vitro toxicity of nitrosamines and nitramines associated with amine-based carbon capture and storage. Environ Sci Technol 48:8203-8211.

22. Fjellsbø LM, Verstraelen S, Kazimirova A, Van Rompay AR, Magdolenova Z, Dusinska M. 2014. Genotoxic and mutagenic potential of nitramines. Environ Res 134:39-45.

23. Goodall CM, Kennedy TH. 1975. Carcinogenicity of dimethylnitramine in NZR rats and NZO mice. Cancer Lett 1:295-298.

24. Mirvish SS, Bulay O, Runge RG, Patil K. 1980. Study of the carcinogenicity of large doses of dimethylnitramine, N-nitroso-L-proline, and sodium nitrite administered in drinking water to rats. J Natl Cancer Inst 64:1435-1442.

25. Scherf H, Frei E, Wiessler M. 1989. Carcinogenic properties of N-nitrodimethylamine and N-nitromethylamine in the rat. Carcinogenesis 10:1977-1981.

26. Hassel M, Frei E, Scherf H, Wiessler M. 1987. Investigation into the pharmacodynamics of the carcinogen N-nitrodimethylamine. IARC Sci Publ 84:150-152.

27. Khudoley V, Malaveille C, Bartsch H. 1981. Mutagenicity studies in Salmonella typhimurium on some carcinogenic N-nitramines in vitro and in the host-mediated assay in rats. Cancer Res 41:3205-3210.

28. Malaveille C, Croisy A, Brun G, Bartsch H. 1983. Hydroxylation and nitroreduction are required to activate dimethyl-nitramine into alkylating and mutagenic agents. Carcinogenesis 4:1477-1481.

29. Frei E, Pool B, Plesch W, Wiessler M. 1984. Biochemical and biological properties of prospective N-nitrodialkylamine metabolites and their derivatives. IARC Sci Publ 57:491-497.

30. Pool BL, Frei E, Plesch WJ, Romruen K, Wiessler M. 1984. Formaldehyde as a possible mutagenic metabolite of N-nitrodimethylamine and of other agents which are suggested to yield non-alkylating species in vitro. Carcinogenesis 5:809-814.

31. Frei E, Pool B, Glatt H, Gemperlein-Mertes I, Oesch F, Schlehofer J, Schmezer P, Weber H, Wiessler M. 1986. Determination of DNA single strand breaks and selective DNA amplification by N-nitrodimethylamine and analogs, and estimation of the indicator cells' metabolic capacities. J Cancer Res Clin Oncol 111:123-128.

32. Suzuki E, Mochizuki M, Sekiguchi N, Osabe M, Okada M. 1985. In vitro metabolism of N-nitrodialkylamines. Jap J Cancer Res 76:28-36.

33. Suzuki E, Mochizuki M, Suzuki T, Okada M. 1986. Metabolic fate of N-nitrodibutylamine in the rat. Jap J Cancer Res 77:39-44.

34. Sørensen L, Zahlsen K, Hyldbakk A, Da Silva EF, Booth AM. 2015. Photodegradation in natural waters of nitrosamines and nitramines derived from CO2 capture plant operation. Int J Greenh Gas Control 32:106-114.

35. Brakstad OG, Sørensen L, Zahlsen K, Bonaunet K, Hyldbakk A, Booth AM. 2018. Biotransformation in water and soil of nitrosamines and nitramines potentially generated from amine-based CO2 capture technology. Int J Greenh Gas Control 70:157-163.

36. Fournier D, Trott S, Hawari J, Spain J. 2005. Metabolism of the aliphatic nitramine 4-nitro-2, 4-diazabutanal by Methylobacterium sp. strain JS178. Appl Environ Microbiol 71:4199-4202.

37. Fournier D, Halasz A, Spain J, Spanggord RJ, Bottaro JC, Hawari J. 2004. Biodegradation of the hexahydro-1, 3, 5-trinitro-1, 3, 5-triazine ring cleavage product 4-nitro-2, 4-diazabutanal by Phanerochaete chrysosporium. Appl Environ Microbiol 70:1123-1128.

38. Miyazaki Y, Kono Y, Shimazu A, Takeuchi S, Yonehara H. 1968. Production of nitraminoacetic acid by Streptomyces noursei 8054-MC3. J Antibiot 21:279-282.

39. Graham DE, Spain JC, Parry RJ, Hettich RL, Mahan KM, Klingeman DM, Giannone RJ, Gulvick CA, Fida TT. 2018. Nitration Enzyme Toolkit for the Biosynthesis of Energetic Materials. Oak Ridge National Lab, Oak Ridge, TN.

40. Borer K, Hardy R, Lindsay W, Spratt D, Mees G. 1966. Ethylene-bis-nitrourethane: Investigation of the plant growth stimulant action of analogous compounds. J Exp Bot 17:378-389.

41. Alston TA, Seitz SP, Porter DJ, Bright HJ. 1980. Inhibition of succinate dehydrogenase by nitroacetate and by the toxic antibiotic nitraminoacetate. Biochem Biophys Res Commun 97:294-300.

42. Mahan KM, Zheng H, Fida TT, Parry RJ, Graham DE, Spain JC. 2017. A novel, iron-dependent enzyme that catalyzes the initial step in the biodegradation of N-nitroglycine by Variovorax sp. strain JS1663. Appl Environ Microbiol 83:e00457-17.

43. Henry JT, Crosson S. 2011. Ligand-binding PAS domains in a genomic, cellular, and structural context. Annu Rev Microbiol 65:261-286.

44. Taylor BL, Zhulin IB. 1999. PAS domains: internal sensors of oxygen, redox potential, and light. Microbiol Mol Biol Rev 63:479-506.

45. Kovaleva E, Neibergall M, Chakrabarty S, Lipscomb JD. 2007. Finding intermediates in the O2 activation pathways of non-heme iron oxygenases. Acc Chem Res 40:475-483.

46. Huang X, Groves JT. 2017. Oxygen activation and radical transformations in heme proteins and metalloporphyrins. Chem Rev 118:2491-2553.

47. Tropea JE, Cherry S, Waugh DS. 2009. Expression and purification of soluble His 6-tagged TEV protease, p 297-307. *In* Doyle SA (ed), Methods in Molecular Biology, vol 498. Springer.

48. Moore S. 2012. Round-the-horn site-directed mutagenesis. Wikiomics.

49. Fish W. 1988. Rapid colorimetric micromethod for the quantitation of complexed iron in biological samples. Methods Enzymol 158:357-364.

50. Stookey LL. 1970. Ferrozine---a new spectrophotometric reagent for iron. Anal Chem 42:779-781.

51. Berry EA, Trumpower BL. 1987. Simultaneous determination of hemes a, b, and c from pyridine hemochrome spectra. Anal Biochem 161:1-15.

52. Bolanos-Garcia VM, Davies OR. 2006. Structural analysis and classification of native proteins from E. coli commonly co-purified by immobilised metal affinity chromatography. Biochim Biophys Acta Gen Subj 1760:1304-1313.

53. Stuffle EC, Johnson MS, Watts KJ. 2021. PAS domains in bacterial signal transduction. Curr Opin Microbiol 61:8-15.

54. Shimizu T, Huang D, Yan F, Stranava M, Bartosova M, Fojtíková V, Martinkova M. 2015. Gaseous O2, NO, and CO in signal transduction: structure and function relationships of heme-based gas sensors and heme-redox sensors. Chem Rev 115:6491-6533.

55. Rao F, Ji Q, Soehano I, Liang Z-X. 2011. Unusual heme-binding PAS domain from YybT family proteins. J Bacteriol 193:1543-1551.

56. Millar S, Moss B, Stevenson M. 1996. Some observations on the absorption spectra of various myoglobin derivatives found in meat. Meat Sci 42:277-288.

57. Enemark J, Feltham R. 1974. Principles of structure, bonding, and reactivity for metal nitrosyl complexes. Coord Chem Rev 13:339-406.

58. William B, Bowen J. 1949. The absorption spectra and extinction coefficients of myoglobin. J Biol Chem 179:235-245.

59. Ford PC. 2010. Reactions of NO and nitrite with heme models and proteins. Inorg Chem 49:6226-6239.

60. Garcia D, Orillard E, Johnson MS, Watts KJ. 2017. Gas sensing and signaling in the PAS-heme domain of the Pseudomonas aeruginosa Aer2 receptor. J Bacteriol 199:e00003-17.

61. Möglich A, Ayers RA, Moffat K. 2009. Structure and signaling mechanism of Per-ARNT-Sim domains. Structure 17:1282-1294.

62. Francis K, Smitherman C, Nishino SF, Spain JC, Gadda G. 2013. The biochemistry of the metabolic poison propionate 3-nitronate and its conjugate acid, 3-nitropropionate. IUBMB Life 65:759-768.

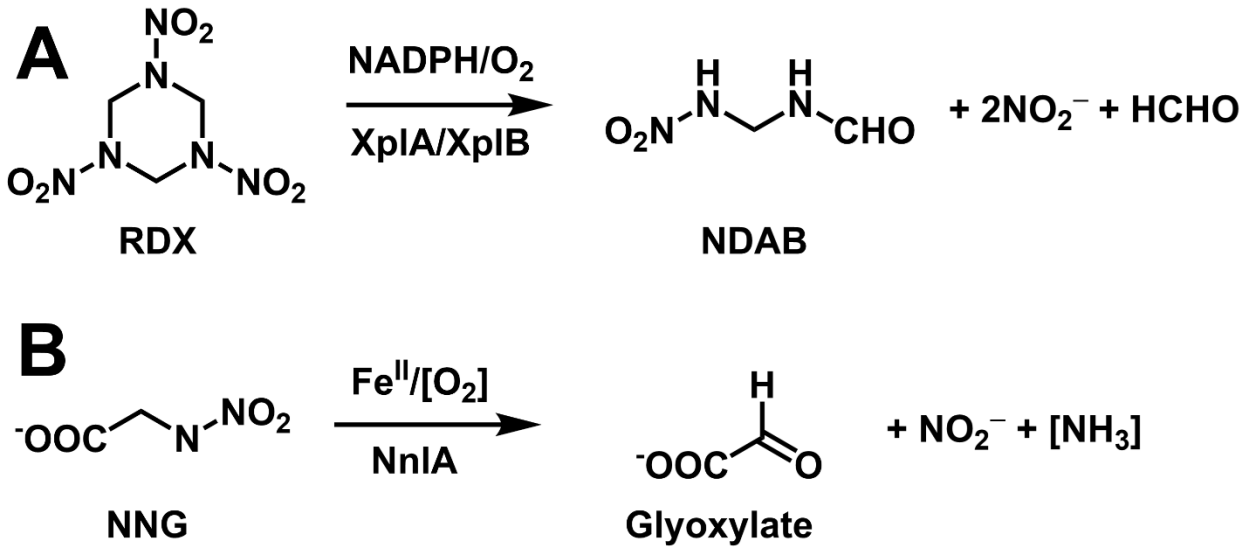

Fig. 1 – Product distributions of nitramine degrading enzymes, including A) aerobic degradation of RDX by XplA and B) degradation of NNG by NnlA. Reactants and products not yet verified are shown in square brackets.

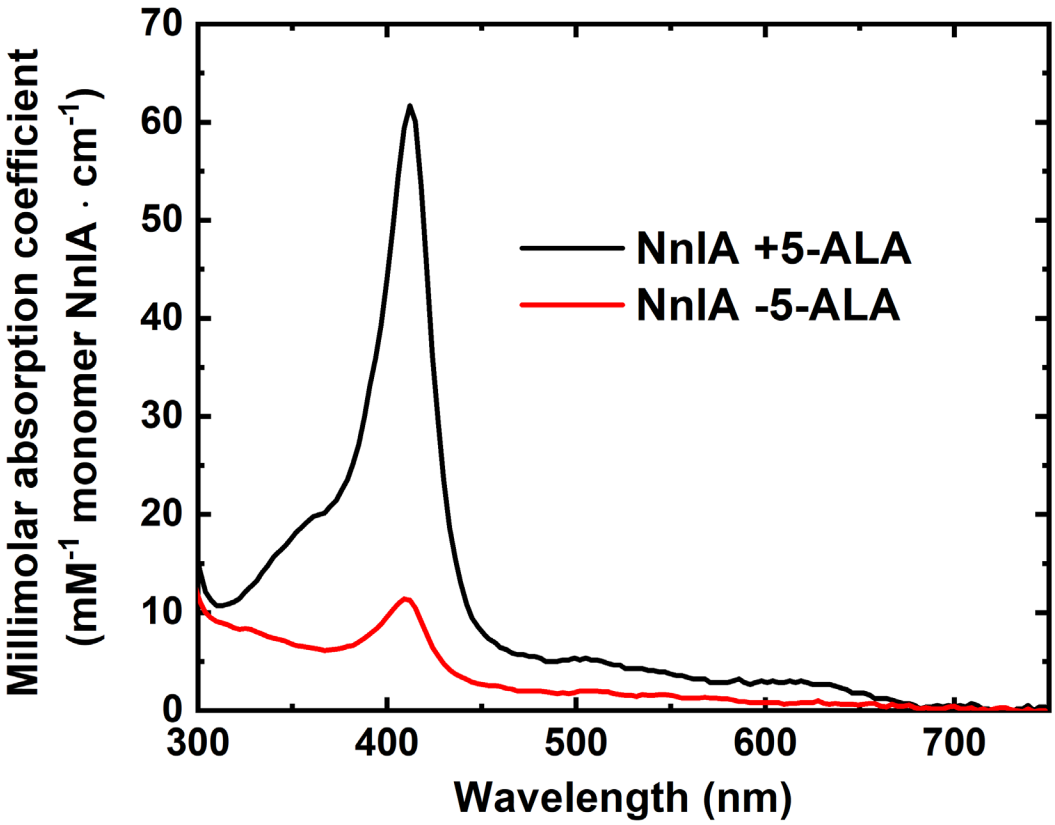

Fig. 2. UV-visible absorption spectra of as isolated NnlA expressed in the absence (red trace) or presence (black trace) of 5-ALA. Both spectra were measured in 50 mM phosphate buffer at pH 7.2.

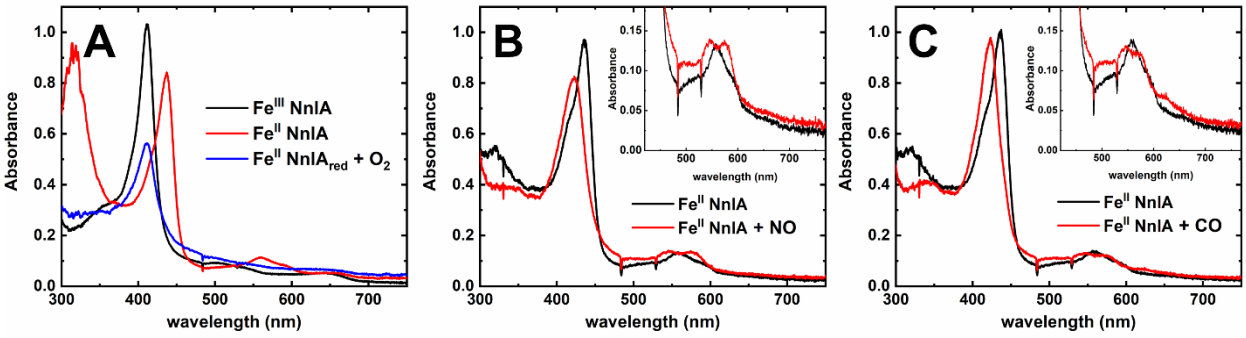

Fig. 3. Treatment of Fe^{II}-NnlA with A) O_2, B) NO or C) CO. Conditions before addition of gas are 10 µM Fe^{II}-NnlA in either in 100 mM Tris-HCl pH 7.6 (panel A) or 100 mM tricine buffer at pH 8 (panels B and C).

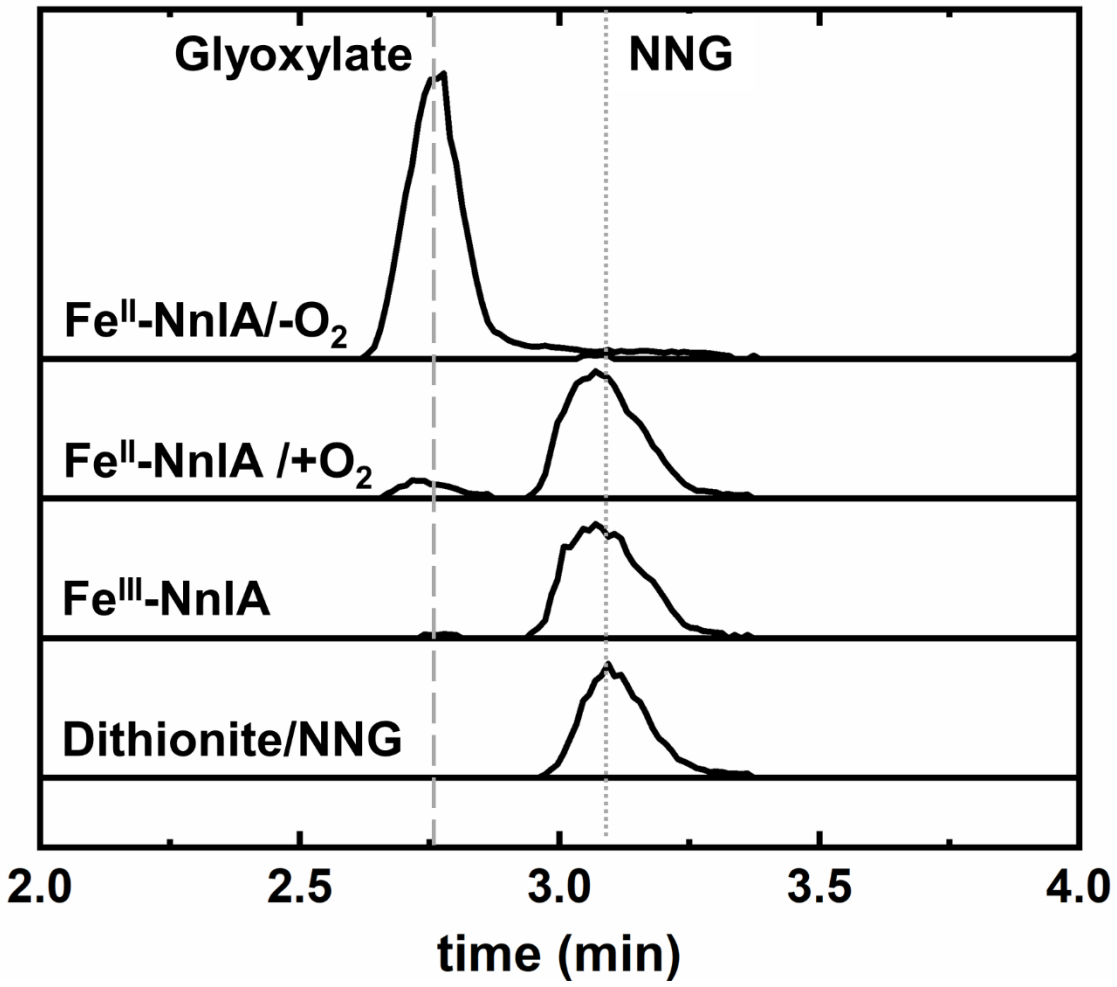

Fig. 4. Overlaid representative LC-MS EICs monitoring molecular anions of NNG (*m*/*z* 119.0) and glyoxylate (*m*/*z* 73.0) in samples containing 500 μM NNG and 10 μM dithionite (Dithionite/NNG), 10 μM as isolated NnlA (Fe^{III}-NnlA), or 10 μM reduced NnlA (Fe^{II}-NnlA). Samples were incubated for 30 minutes at room temperature in deoxygenated 20 mM phosphate buffer, pH 7.2. The Fe^{II}-NnlA/O_2 sample was incubated in air-saturated buffer. Dashed and dotted gray lines indicate elution time of glyoxylate and NNG in standard solutions.

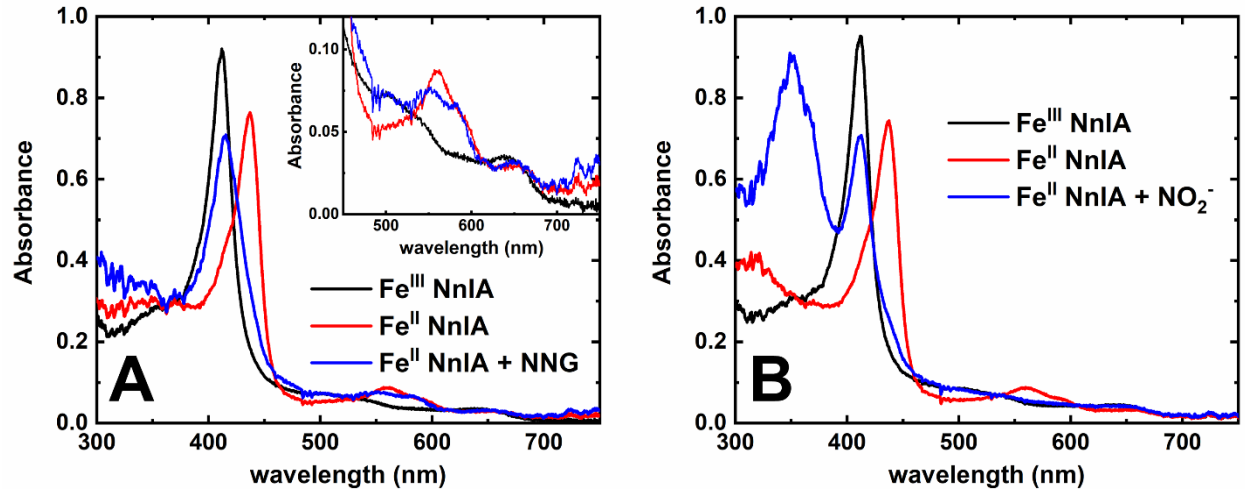

Fig. 5 – UV-visible spectra of reduced NnlA treated with either NNG (Panel A) or NO_2^- (Panel B) under anaerobic conditions. Reaction conditions: (Panel A) 3 μM Fe^{II}-NnlA, 133 μM NNG, in deoxygenated 20 mM phosphate, pH 7.5 incubated for 5 hours at room temperature; (Panel B) 3 μM Fe^{II}-NnlA with 133 μM NO_2^- in deoxygenated 20 mM phosphate, pH 7.5 at room temperature.

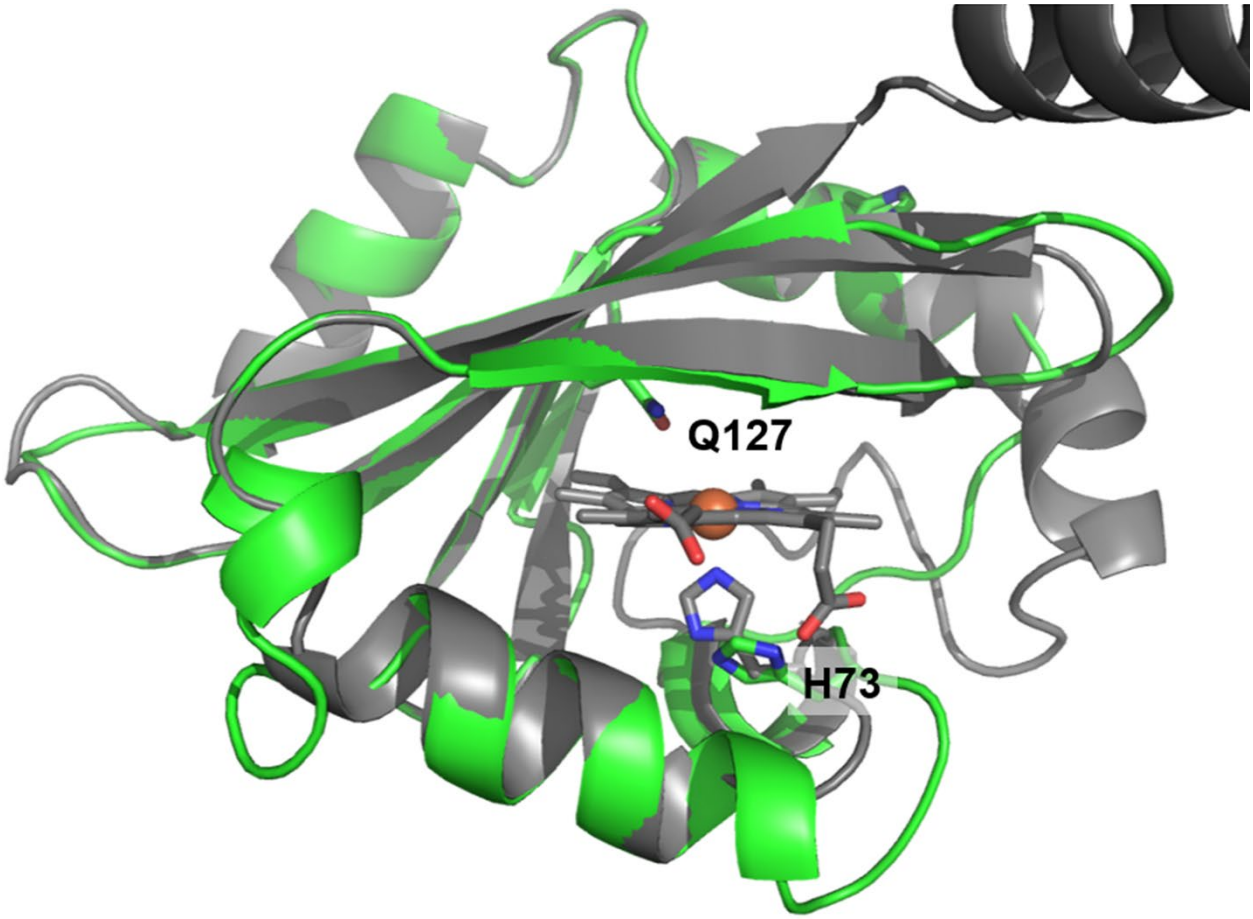

682

683 **Fig. 6**. Structural homology model of NnlA overlayed on the crystal structure of the CN^-

684 complexed PAS domain from *Pa* Aer2 (PDB: 3VOL; grey). Peptide backbone of NnlA structural

685 homology model shown as green cartoon and *Pa* Aer2 backbone shown as grey cartoon. Iron

686 atom shown as orange sphere, oxygen and nitrogen atoms shown in red and blue, respectively.

687 Structural homology model was generated by SWISS-MODEL.

688

689

690

691

692

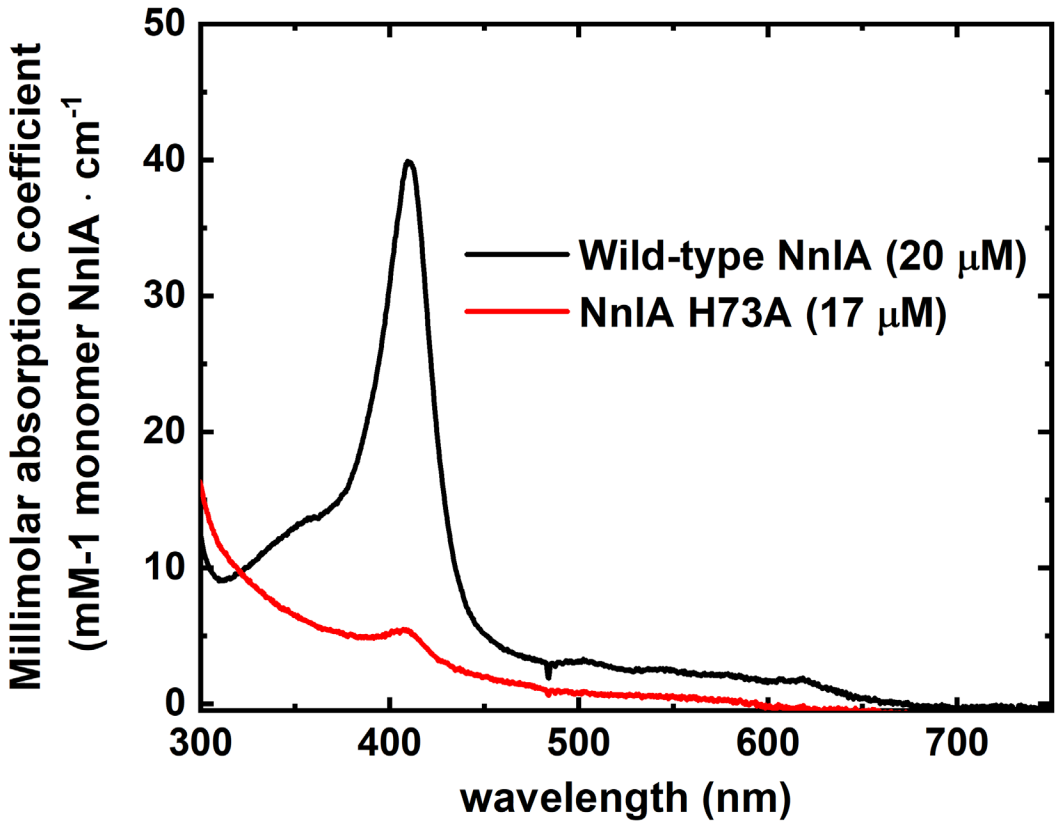

Fig. 7 – UV-visible absorption spectra of 20 μM wild-type or 17 μM H73A NnlA. All samples prepared in 100 mM tricine buffer, pH 8.

Schemes

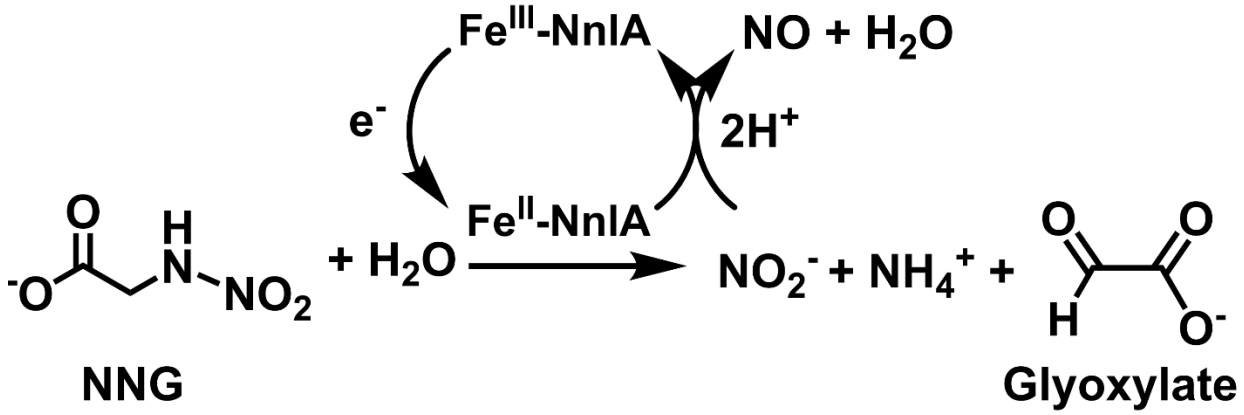

Scheme 1. Summary of NnlA activity.

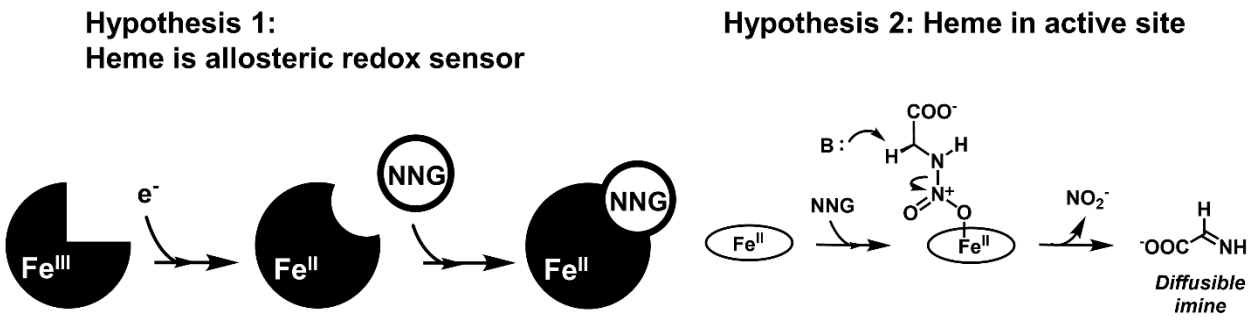

Scheme 2. Proposed roles of heme cofactor in NnlA.